Investigation of the mechanisms underpinning plasma-catalyst interaction for

the conversion of methane to oxygenates

Jingkai Jiang and Peter J. Bruggeman\*

Department of Mechanical Engineering, University of Minnesota, 111 Church Street SE,

Minneapolis 55414 Minnesota, United States of America

\*email: pbruggem@umn.edu

Abstract

Plasma catalysis is a promising approach to further enhance the conversion of methane into value-

added products such as methanol. In this work, the mechanisms enabling the conversion of

methane to CO, CO<sub>2</sub> and methanol enabled by plasma-enhanced catalysis were investigated. A

catalyst reactor was incorporated downstream of the plasma jet to enable the separation between

plasma generation and the catalyst bed. An enhancement in CH<sub>3</sub>OH and CO<sub>2</sub> production was

observed for the shortest distance between the plasma and catalyst compared to the plasma-only

case. Plasma-enabled gas heating was shown not to be responsible for the observed synergy while

a gas temperature increase as low as 30-40 K significantly impacted desorption rates of

CH<sub>3</sub>OH/C<sub>2</sub>H<sub>5</sub>OH on alumina particles. Correlations between molecular beam mass spectrometry

(MBMS) measurements at the inlet and outlet of the catalytic reactor suggest that the observed

synergistic effect was caused by radical species most likely the CH<sub>3</sub>O<sub>2</sub> radical. This study shows

that surface reactions induced by radicals such as alkylperoxy radicals might play an important

role in surface reactions in plasma-catalysis.

**Key words:** Partial oxidation of methane, oxygenates, APPJ, molecular beam mass spectrometry

1. Introduction

Catalytic partial oxidation of CH<sub>4</sub> is a particularly interesting route for converting the abundantly

available natural gas into higher energy density liquid fuels [1]. Methanol (CH<sub>3</sub>OH), one of the

products of partial CH<sub>4</sub> oxidation, is furthermore a clean and renewable fuel source and is also in

great demand as an intermediate source of green energy to provide electric energy generation via

fuel cell technology applications [2].

The conventional approach to convert CH<sub>4</sub> into CH<sub>3</sub>OH is a two-step catalytic process. The first step is to convert CH<sub>4</sub> into syngas (CO + H<sub>2</sub>) at high temperatures. The syngas is subsequently converted to methanol or other liquid fuels at high temperature and pressures (typically 60–100 bar and 250–280 °C) over a Cu–ZnO-based catalyst. Due to the high cost of this process, alternative energy-efficient technologies to directly convert CH<sub>4</sub> into CH<sub>3</sub>OH or other oxygenates are being developed based on the partial oxidation of methane.

$$CH_4 + \frac{1}{2}O_2 \rightarrow CH_3OH, \Delta H_{298K}^0 = -126.2 \text{ kJ mol}^{-1}$$
 (R1)

Although significant efforts have been devoted to the investigation of direct conversion of methane to oxygenates via thermal catalysis, the reported product yields in terms of CH<sub>3</sub>OH to date are insufficient to replace the conventional two-step process [3]. Plasma-catalysis has been proposed as an innovative approach to enable methane to methanol conversion. This approach exploits the observed synergistic effect between plasma and thermal catalysis that potentially enables chemical conversion at lower temperatures and pressures as in conventional thermal catalytic processes [4].

Nozaki and Okazaki [5] experimentally and theoretically analyzed the energy efficiency of nonoxidative methane conversion using a dielectric barrier discharge (DBD), and showed an enhanced CH<sub>4</sub> conversion efficiency attributed to vibrationally excited species. Kim et al. [6] performed a detailed kinetic study of CH4 activation in a DBD to quantify plasma-catalyst interactions via kinetic parameters. The results showed that the thermal catalysis had a typical Arrhenius behavior with an activation energy of ~73.5 kJ mol<sup>-1</sup>, while the plasma catalysis case exhibited non-Arrhenius behavior suggested to be due to the interaction between plasma and catalysts. In addition, the reported energy barrier for plasma catalysis was found to be much lower than the activation energy needed in thermal catalysis. The same group reported on the dry reforming of CH<sub>4</sub> with CO<sub>2</sub> using Ni/Al<sub>2</sub>O<sub>3</sub> catalysts, and showed a significant enhancement of the activation of C-H bonds by the plasma when the gas temperature > 630 K [7]. The comparison between the CH<sub>4</sub> conversions of thermal catalysis and plasma catalysis indicated a ~50 K shift in the activation energy. This 50 K gas temperature increase could be easily caused by localized plasma-induced gas heating. In addition to these synergistic effects, the use of non-thermal plasmas for catalyst regeneration was also reported [8]. The active species produced by the plasma can oxidize the coke formed on the catalyst and regenerate the catalyst at room temperature (293 K), requiring potentially lower energy than the common thermal regeneration requiring ~800 K.

Recently, Chawdhury et al. [9] investigated the plasma-catalytic partial oxidation of methane into oxygenates in a dielectric barrier discharge (DBD) reactor at room temperature. Three different supported transition metal catalysts ( $N_i/\gamma$ - $Al_2O_3$ ,  $Cu/\gamma$ - $Al_2O_3$ , and  $Fe/\gamma$ - $Al_2O_3$ ) were tested, and the result showed that Fe/y-Al<sub>2</sub>O<sub>3</sub> provided the highest methanol selectivity (36%) and a methanol yield of 4.7%. The authors suggested that plasma-produced CH<sub>x</sub> species were critical for CH<sub>3</sub>OH production. De Bie et al. [10] established a one-dimensional fluid model of a DBD reactor to model the conversion of methane into oxygenates. The main underlying reaction pathways forming syngas, methanol and other oxygenates were determined for both partial oxidation and dry reforming of methane. The formation of methanol in the gas phase was shown to be due to radical reactions involving CH<sub>3</sub>, CH<sub>3</sub>O<sub>2</sub> and CH<sub>3</sub>O as the main intermediate species. Yi et al. [11] investigated the selective oxidation of CH<sub>4</sub> to CH<sub>3</sub>OH over Ni-based catalysts at low temperature and atmospheric pressure and achieved 81% oxygenate selectivity and 50 % CH<sub>3</sub>OH selectivity. This work also reported kinetic modelling results with similar conclusions as De Bie et al. [10] The production of CH<sub>3</sub>OH on the catalyst was however attributed to chemisorbed oxygen species that react with the plasma-produced gas-phase CH<sub>3</sub> radicals to form the intermediate species CH<sub>3</sub>O<sub>ad</sub> on the catalyst. The authors also hypothesized that H<sub>2</sub>O molecules produced by the plasma might be activated by the NiO/γ-Al<sub>2</sub>O<sub>3</sub> catalyst and then further promote the desorption of CH<sub>3</sub>OH from the catalyst surfaces, according to the findings from [12].

Although researchers have successfully increased CH<sub>3</sub>OH yields in plasma catalysis reactors by adjusting the composition of catalysts and plasma conditions, such findings require trial-and-error parametric studies and our understanding of the underpinning process remains limited. This lack of understanding hampers further improvements in energy efficiencies, selectivity and yield for CH<sub>3</sub>OH production by plasma catalysis. Inspired by the work of Chawdhury et al. [9] we implemented a detailed study of plasma-produced species and conversion yields to investigate the plasma-catalyst interaction in the context of direct conversion of methane to oxygenates at room temperature. This is enabled by decoupling the catalyst and the plasma reactor similarly as in [13]. The products and plasma-produced species with or without catalysts were both quantified using molecular beam mass spectrometry (MBMS). Plasma-produced reactive species entering the catalytic reactor were correlated with the products downstream of the catalyst reactor to assess their importance in the plasma-catalyst interaction.

### 2. Experimental setups

### 2.1 Plasma jet and catalyst reactor

In this work, we coupled an atmospheric pressure plasma jet with a catalytic reactor downstream enabling the separation of the active plasma region and catalyst, as shown in figure 1. As the catalyst reactor can be detached from the plasma jet, this configuration also allowed us to measure the species densities both at the entrance and exit of the catalytic reactor. We used three different combinations of the plasma jet and the catalyst reactor, as shown in figure 1. These configurations allow for distinguishing effects of short-lived species and long-lived species by investigating two distances from the plasma jet electrode to the catalysis reactor (5 mm and 33 mm, respectively).

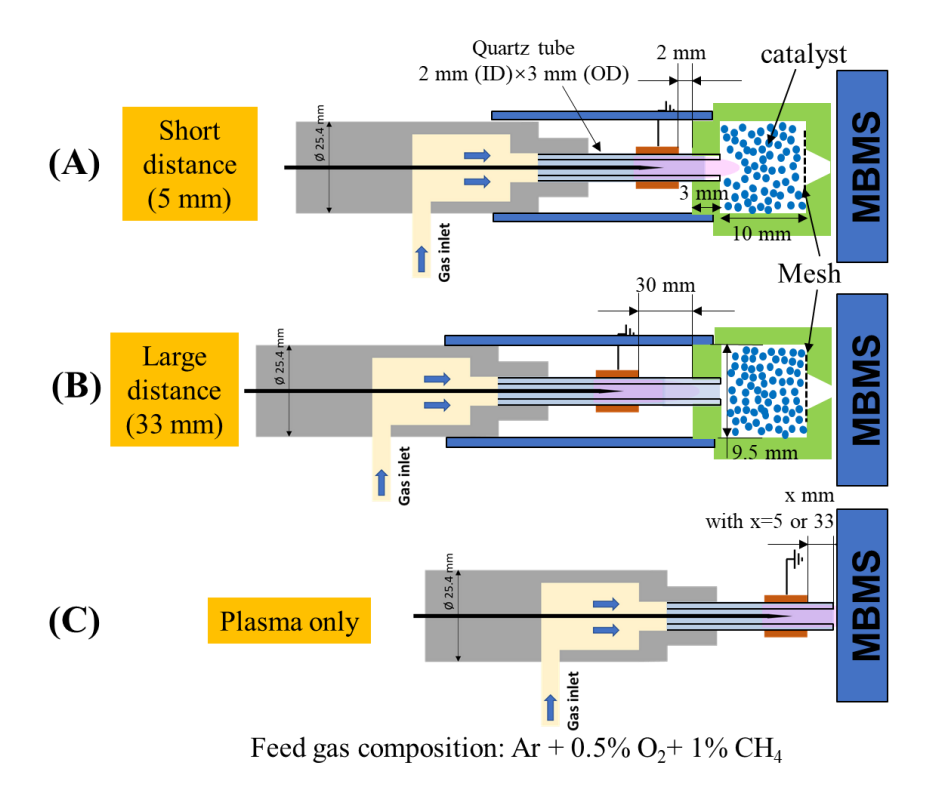


**Figure 1.** Schematic of the different configurations of the flow-through plasma-catalysis reactor used in this study.

The plasma jet used in this work is identical to the one used in [13]. The plasma jet was driven by a radiofrequency voltage waveform modulated by a 20 kHz modulation with a 20% duty cycle. The main difference with the work in [13] is that CH<sub>4</sub> is added into the feed gas instead of being

mixed downstream in the plasma effluent. The composition of the feed gas was fixed at Ar + 1% CH<sub>4</sub> + 0.5% O<sub>2</sub> throughout this study. The Ar flow rates were kept constant at 200 sccm in this study unless otherwise stated. Higher CH<sub>4</sub>/O<sub>2</sub> ratios as used in [9] were also attempted in the preliminary experiments but resulted in carbon deposition or gas-phase carbon particle formation, which was not further pursued to avoid clogging of the sampling orifice of the MBMS. A 200 mesh was implemented at the outlet of the catalyst reactor to prevent the catalyst particles from being blown out and similarly blocking the sampling orifice of the MBMS. The operation of the plasma jet and the plasma dissipated power calculation are described in detail elsewhere [14]. The gas temperature measurements in this study were performed with a K-type thermal couple or a temperature strip (OMEGA, RLC) with a temperature resolution of 5 K.

### 2.2. Catalyst information and preparation

Microsphere catalysts (20% wt% Fe/ $\gamma$ -Al<sub>2</sub>O<sub>3</sub>) and the control group  $\gamma$ -Al<sub>2</sub>O<sub>3</sub> particles from Riogen, Inc. were used in this study. All the particles have the same size (~375  $\mu$ m), and the entire catalytic reactor was loaded loosely without compressing the catalyst to ensure a low flow resistance. The weights of the loaded Fe/ $\gamma$ -Al<sub>2</sub>O<sub>3</sub> and Al<sub>2</sub>O<sub>3</sub> particles were 0.53 g and 0.39 g, respectively. The pretreatment consisted of an Ar+4% H<sub>2</sub> plasma treatment at atmospheric pressure for about 2 hours after the catalyst reactor was installed in the reactor.

#### 2.3 Molecular beam mass spectrometry (MBMS)

MBMS was used to quantify the reactive species produced by the plasma as well as the downstream products of the catalyst reactor. The details of the MBMS system used can be found in [15]. The species measured in this work include the reactants (CH<sub>4</sub> and O<sub>2</sub>), main products (CO, CO<sub>2</sub>, H<sub>2</sub>), minor products (oxygenates) and the short-lived species CH<sub>3</sub>. While attempted, we were unable to measure atomic oxygen and hydrogen radicals. **Table 1** provides a summary of the electron energy and calibration gas used for each species measured by MBMS.

**Table 1.** Summary of electron energies and calibration gases for each species by MBMS. A reference to work reporting the method or electron ionization cross sections used for threshold ionization mass spectrometry is also provided for species that are not calibrated with known concentrations of the species itself.

Species name	Tracked species mass m/z (amu)	MBMS electron energy (eV)	MBMS calibrated gas	Ref.
CH <sub>3</sub> /CH <sub>3</sub> O <sub>2</sub>	15	12.5	CH4	[16]–[19]
CH <sub>3</sub> OH or C <sub>2</sub> H <sub>5</sub> OH	31	70	O <sub>2</sub>	[17],[20]
C <sub>2</sub> H <sub>6</sub> or CH <sub>2</sub> O	30	70	$N_2$	[17]
C <sub>2</sub> H <sub>5</sub> OH or HCOOH	46	70	None	[17],[21]
CH <sub>3</sub> COCH <sub>3</sub>	58	70	None	[22]
CH <sub>3</sub> COOH	60	70	None	[23]
CO	28	70	$N_2$	[17]
$CO_2$	44	70	$CO_2$	
H <sub>2</sub>	2	70	$H_2$	
$O_2$	32	70	$O_2$	
CH <sub>4</sub>	15	70	CH <sub>4</sub>	

The measurements of stable species including CO, CO<sub>2</sub>, H<sub>2</sub>, O<sub>2</sub>, and CH<sub>4</sub> have been performed using electron energy of 70 eV. Their absolute calibration also is straightforward because it can be achieved with a known concentration of the particular gas. For the short-lived reactive species, threshold ionization mass spectrometry (TIMS) is used to exclude the contribution of dissociative ionization from their parent molecules. An additional 50 Hz RF plasma modulation is implemented on top of the 20 kHz RF modulation to enable the accurate subtraction of the background signals. Details regarding the TIMS and the rationale and implementation of the background subtraction approach can be found in [15]. We were only able to measure a radical signal at 15 amu. A detailed analysis in the result section shows that this cannot be due to the methyl radical as initially expected but is due to the CH<sub>3</sub>O<sub>2</sub> radical. We have also measured m/z=47 corresponding to CH<sub>3</sub>O<sub>2</sub><sup>+</sup> which yielded similar trends as CH<sub>3</sub><sup>+</sup> although with lower signals likely because CH<sub>3</sub>O<sub>2</sub><sup>+</sup> is an unstable ion [18]. We have for this reason used the CH<sub>3</sub><sup>+</sup> signal (see results section for more details).

The possible oxygenates produced in this work include methanol (CH<sub>3</sub>OH), ethanol (C<sub>2</sub>H<sub>5</sub>OH), formaldehyde (CH<sub>2</sub>O), formic acid (HCOOH), acetic acid (CH<sub>3</sub>COCH<sub>3</sub>), and acetone (CH<sub>3</sub>COCH<sub>3</sub>). Due to the possible existence of other hydrocarbons with the same masses such as C<sub>2</sub>H<sub>6</sub> and the complex cracking pattern of these oxygenates in the mass spectrum, further analysis of the MBMS results is required. According to the mass spectrum of oxygenates and relative hydrocarbons, the masses (m/z=60 amu and m/z=58 amu) can represent formic acid and acetic acid, respectively. The mass (m/z=46 amu) is a combination of ethanol and formic acid, and the mass (m/z=30 amu) can represent both C<sub>2</sub>H<sub>6</sub> and CH<sub>2</sub>O.

As for CH<sub>3</sub>OH with a mass of 32 amu, we tracked the fragment (m/z=31 amu) which is the highest signal at 70 eV in the CH<sub>3</sub>OH mass spectrum, as this enables to exclude the contribution from the abundantly present O<sub>2</sub> molecules which have the same mass as methanol. Nevertheless, ethanol (C<sub>2</sub>H<sub>5</sub>OH) might also contribute significantly to the mass (m/z=31). Contributions of other oxygenates to the m/z=31 is less likely as this fragment is less abundant (<1%) for other oxygenates at 70 eV. Hence the measured species with mass of 31 represent CH<sub>3</sub>OH or C<sub>2</sub>H<sub>5</sub>OH. The partial cross-sections of CH<sub>3</sub>O<sup>+</sup> from CH<sub>3</sub>OH and C<sub>2</sub>H<sub>5</sub>OH at 70 eV are 1.5×10<sup>-16</sup> cm<sup>-3</sup> and 2.5×10<sup>-16</sup> cm<sup>-3</sup>, respectively [20] and require further analysis for distinguishing between the two species.

In this work, the percentage conversion ( $\eta$ ) of CH<sub>4</sub> and O<sub>2</sub> are calculated as:

CH<sub>4</sub>/O<sub>2</sub> conversion (%)= 
$$\eta = \frac{\text{Converted} \frac{\text{CH}_4}{\text{O}_2} \text{molecules at the reactor exhaust}}{\text{Total} \frac{\text{CH}_4}{\text{O}_2} \text{molecules at the reactor input}} \times 100.$$
 (1)

The production rates of species are calculated as:

production rate 
$$(s^{-1}) = n_i \cdot \Phi$$
, (2)

with  $n_i$  the measured species density of species i at the exit of the reactor and  $\Phi$  the volumetric gas flow rate.

The conversion rate of CH<sub>4</sub> and O<sub>2</sub> are calculated as:

conversion rate 
$$(s^{-1}) = \eta \cdot n_i \cdot \Phi$$
, (3)

with  $n_i$  the density of CH<sub>4</sub> and O<sub>2</sub> in the feed gas entering the reactor.

#### 3. Results and discussion

# 3.1. CH<sub>4</sub> and O<sub>2</sub> conversion by plasma and product identification

In this section, a general overview of the CH<sub>4</sub> and O<sub>2</sub> conversion as well as the main products for the plasma without catalyst case are provided as a reference for the plasma catalysis results reported in later sections. Figure 2 (a) shows the CH<sub>4</sub> and O<sub>2</sub> conversion as a function of plasma dissipated power. The influence of gas temperature is minimized by performing the measurements with an extended quartz tube (30 mm) which keeps the gas temperature near room temperature (below 340 K) at the nozzle. As both CH<sub>4</sub> and O<sub>2</sub> are flowing through the ionizing plasma region, CH<sub>4</sub> and O<sub>2</sub> conversions up to 30% and 50% respectively are observed in the investigated power range. The conversion of both CH<sub>4</sub> and O<sub>2</sub> increases with increasing plasma dissipated power.

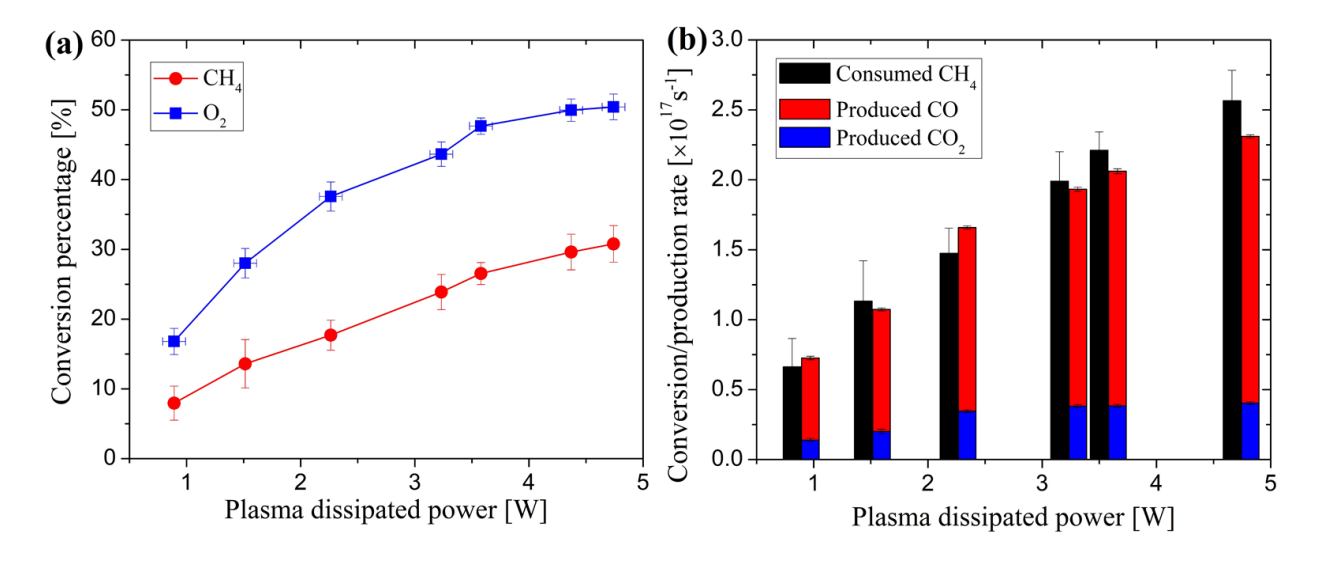


**Figure 2.** (a) CH<sub>4</sub> and O<sub>2</sub> conversions as a function of plasma dissipated power for the plasma only (case C in Figure 1); (b) Conversion rate of CH<sub>4</sub> and associated production rate of CO and CO<sub>2</sub>.

Figure 2 (b) compares the conversion rate of CH<sub>4</sub> with the production rate of CO and CO<sub>2</sub>, the dominant carbon-containing products. Comparing the combined CO and CO<sub>2</sub> production rate with the CH<sub>4</sub> conversion rate indicates that more than 90% of the CH<sub>4</sub> is converted into CO and CO<sub>2</sub>, with CO accounting for about ~80% of the CH<sub>4</sub> conversion. As shown below, the H<sub>2</sub> production rate is similar to the CO production rate, hence based on stoichiometric considerations the H<sub>2</sub>O production rate, which is more challenging to measure is also to be expected similar to the CO

production. This also means that the selectivity of hydrocarbon to oxygenate conversion by the RF plasma jet is below  $\sim 10\%$  and seems to be favored for higher plasma powers.

To quantify the oxygenates produced by the plasma, measurements of methanol/ethanol (CH<sub>3</sub>OH/C<sub>2</sub>H<sub>5</sub>OH), formaldehyde (CH<sub>2</sub>O), formic acid (HCOOH), acetic acid (CH<sub>3</sub>COOH) and acetone (CH<sub>3</sub>COCH<sub>3</sub>) were performed with the MBMS. Figure 3(a) shows time-resolved measurements of the mass corresponding to several oxygenates with an electron energy of 70 eV. The partial ionization cross-sections at 70 eV of these measured fragments from oxygenates are all within a factor of 2 and on the order of 10<sup>-16</sup> cm<sup>2</sup> [20]–[23]. Nonetheless, smaller molecules would have larger losses during the supersonic expansion and molecular beam [24] than heavier molecules although their ionization cross-sections are generally smaller as well which will compensate to some extent for this difference. Hence, the relative mass spectrometry signals represent within approximately a factor 2 the concentration of each oxygenate. The MS signal is corrected for background contributions by subtracting the MS signal collected during 'plasma off' for the oxygenates.

Figure 3(b) shows that methanol/ethanol (m/z=31) has the largest signal (difference between plasma ON and OFF) compared to the other measured oxygenates. Both CH<sub>3</sub>COOH and CH<sub>3</sub>COCH<sub>3</sub> are approaching the detection limit and are not analyzed in detail. To further evaluate the contribution of C<sub>2</sub>H<sub>5</sub>OH to the measured signals (m/z=31), we compared the signals at m/z=45 and m/z=46. At electron energy of 70 eV, the ratios of fragments at m/z=45 and m/z=46 for C<sub>2</sub>H<sub>5</sub>OH and HCOOH are about 2.5 and 0.8, respectively [25]. Based on this fragment ratio (~2.0 in our experiments), a rough estimation of the density ratio of C<sub>2</sub>H<sub>5</sub>OH and HCOOH can be obtained, which is about 7:3. Furthermore, with this density ratio of C<sub>2</sub>H<sub>5</sub>OH and HCOOH, the contribution from C<sub>2</sub>H<sub>5</sub>OH to the signal at m/z=31 can be estimated, which is about 30%. In addition, the signals at m/z=30 are about 70% of that at m/z=31, which might be interpreted as formaldehyde (CH<sub>2</sub>O) or C<sub>2</sub>H<sub>6</sub> but these two species are not distinguishable. The experimental results from [9] indicated that the CH<sub>2</sub>O density might be comparable to that of C<sub>2</sub>H<sub>6</sub>.

The above comparison shows that CH<sub>3</sub>OH is the most dominant oxygenate produced by the plasma. Therefore, we focus on m/z=31 for the investigation of oxygenates in this study while recognizing that C<sub>2</sub>H<sub>5</sub>OH contributes to the MS signal.

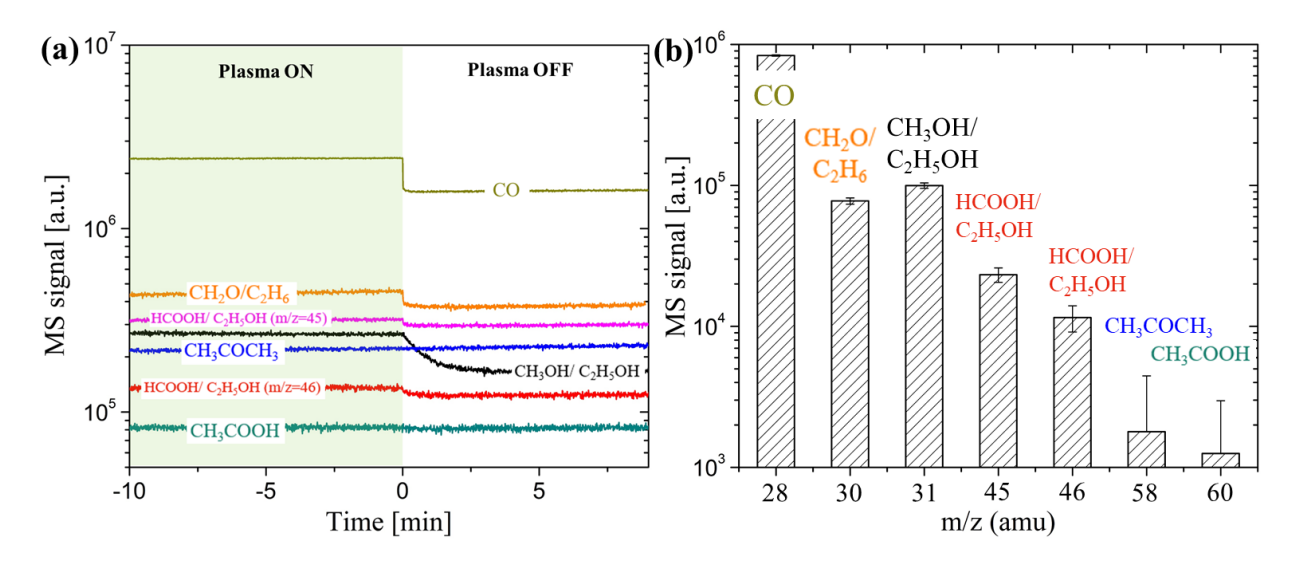


**Figure 3.** (a) Time-resolved mass spectrometry signals for CO and different oxygenates; (b) comparison of mass spectrometry signals (the difference between plasma ON and plasma OFF) for CO and different oxygenates. The plasma power was 4.7 W and the distance between the electrode and the nozzle was 5 mm.

## 3.2. Comparison of plasma with and without catalyst

The observed synergy in plasma catalysis is recently becoming more and more attributed to radicals [11],[26] although this attribution is typically based on indirect observations. To assess the role of short-lived species in plasma-catalyst interactions, we investigated in this study the two configurations in figure 2 which enabled us to study plasma-catalyst interactions for a distance of 5 and 33 mm between the electrode and the entrance of the catalytic reactor.

As the plasma plume length for the maximum power case is less than 5 mm, the case of 33 mm has at least a 28 mm distance between the plasma and catalyst particles. Given that for the reference flow rate of 200 sccm, this distance corresponds to a gas residence time of 26 ms short-lived plasma-produced radicals will not reach the catalytic reactor although the impact of long-lived reactive plasma-produced species onthe catalysts can be assessed. Indeed radicals such as CH<sub>3</sub>, O, H and CH<sub>3</sub>O<sub>2</sub> have for the conditions and gas composition investigated in this work lifetimes of at most 1 ms (see also futher). In the case of 5 mm, the catalyst and the plasma remain separated (no direct coupling) but when the plasma power is increased the tip of the plasma plume can reach the entrance of the catalyst reactor. This might enable a more complex interaction between the plasma and the catalyst, and a fraction of the plasma-produced radicals will reach the catalyst particles

before recombining. While Ar plasmas are known to produce excimer radiation and argon metastable species that have the potential to impact catalytic surface reactions, the presence of O<sub>2</sub> and CH<sub>4</sub> in excess of 1 % of the total gas composition reduces the lifetimes of the Ar excited states by reactions with molecules. This leads to dissociation of O<sub>2</sub> and CH<sub>4</sub> and the production of radicals while the metastable density become very low and the excimer production is suppressed [27],[28]. Hence, CH<sub>4</sub> and O<sub>2</sub> chemistry will dominate under the investigated conditions.

## 3.2.1. CH<sub>4</sub> and O<sub>2</sub> conversion

Figure 4 compares the CH<sub>4</sub> and O<sub>2</sub> conversion as a function of plasma power with catalyst particles or with alumina particles (configuration A and B in Figure 1) to evaluate potential synergistic effects. Nonetheless, the CH<sub>4</sub> conversion is identical within the experimental uncertainty (~5×10<sup>15</sup> cm<sup>-3</sup>) for the four cases suggesting that the addition of a catalyst does not enhance the CH<sub>4</sub> conversion for the investigated conditions. On the other hand, an enhancement of the O<sub>2</sub> conversion was observed at higher plasma powers for the 5 mm case (configuration A in Figure 1) where radicals are able to reach the catalyst (see further). Considering that the enhancement in CH<sub>4</sub> conversion is negligible, it suggests an increase in oxygen-containing products, possible oxygenates or CO<sub>2</sub>.

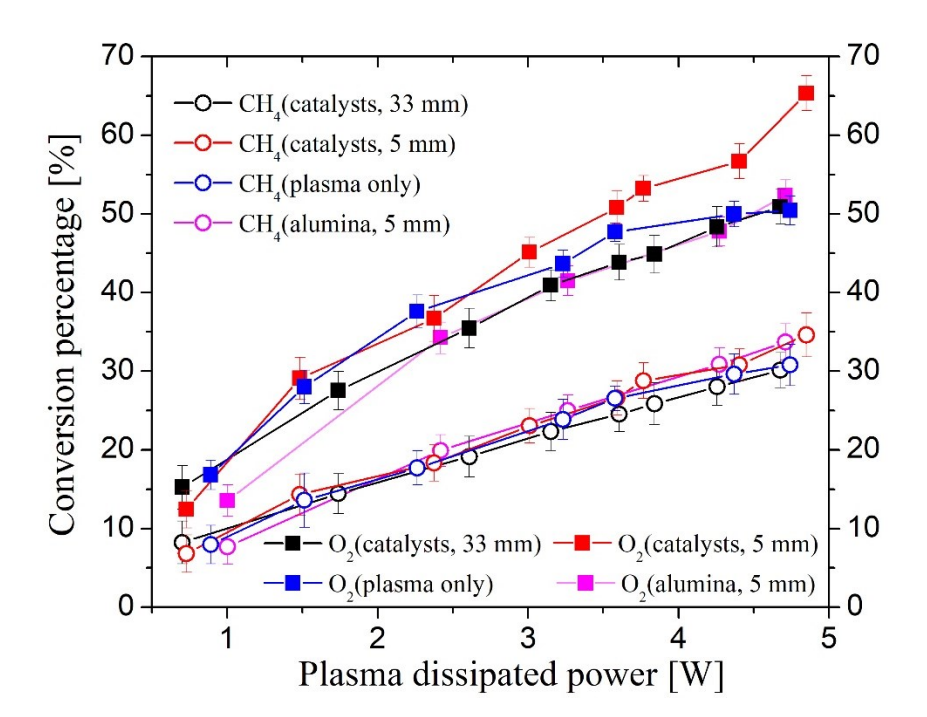


**Figure 4.** Comparison of CH<sub>4</sub> and O<sub>2</sub> conversion as a function of plasma dissipated power for plasma only (configuration C in Figure 1) and plasma-catalysts at a distance of 5 and 33 mm (configuration A and B in Figure 1, respectively). A case where the catalyst was replaced with alumina pellets at a distance of 5 mm was also included as a reference.

#### 3.2.2. Products

Figures 5 (a)-(d) show the densities of the dominant conversion products (H<sub>2</sub>, CO, CO<sub>2</sub> and CH<sub>3</sub>OH/C<sub>2</sub>H<sub>5</sub>OH) as a function of plasma dissipated power for the same experimental conditions as the CH<sub>4</sub> and O<sub>2</sub> conversion shown in Figure 4. The introduction of the catalyst does not impact the H<sub>2</sub> and CO production significantly. Nonetheless, a significant increase in CO<sub>2</sub> production is observed for the 5 mm case (configuration A in Figure 1) in the presence of catalysts compared to the other cases for powers in excess of 4 W. This increase in CO<sub>2</sub> density of ~0.7×10<sup>16</sup> cm<sup>-3</sup> correlates with the observed increase in O<sub>2</sub> conversion at higher plasma power as shown in Figure 4. As the increase is not found for alumina pellets without catalyst, the increase of CO<sub>2</sub> is enabled by the presence of the catalyst in the plasma effluent, as discussed in detail [13]..

Figure 5(d) shows the methanol/ethanol production which interestingly, shows two obvious different trends for low and high plasma powers. The 'plasma only' case can be considered representative for the CH<sub>3</sub>OH/C<sub>2</sub>H<sub>5</sub>OH production by the plasma and CH<sub>3</sub>OH/C<sub>2</sub>H<sub>5</sub>OH species entering the catalytic reactor. While the CH<sub>3</sub>OH/C<sub>2</sub>H<sub>5</sub>OH densities do not show a strong dependence on the plasma dissipated power, = at larger plasma powers, the CH<sub>3</sub>OH density decreases likely due to the dissociation of the formed CH<sub>3</sub>OH in the ionizing plasma. The following sections mostly focus on the explanation of these two changes.

At small plasma powers (1-2.5 W), the addition of catalyst and alumina particles leads to a remarkable reduction in the measured CH<sub>3</sub>OH/C<sub>2</sub>H<sub>5</sub>OH density. This reduction is caused by the fact that it takes up to 3-4 hours for the system to reach a steady state. We studied this effect in the case of alumina in detail and showed that once the plasma-catalyst system reaches steady-state it yields, within the experimental accuracy, the same amount of CH<sub>3</sub>OH/C<sub>2</sub>H<sub>5</sub>OH as in the 'plasma only' case. It was further confirmed that at larger plasma powers the system reaches a steady state on a timescale  $\sim 10\,$  minutes and the CH<sub>3</sub>OH/C<sub>2</sub>H<sub>5</sub>OH losses to the alumina causing this effect do not have an impact on the reported measurements. Hence, the increase found for the 5 mm case with catalyst suggests a plasma-catalyst synergy which is analyzed in more detail below. It should

be noted that this synergy cannot be readily explained by conversion of plasma-produced syngas into CH<sub>3</sub>OH/C<sub>2</sub>H<sub>5</sub>OH as the 33 mm case (configuration B in Figure 1) does not yield an enhancement of CH<sub>3</sub>OH/C<sub>2</sub>H<sub>5</sub>OH. In the next section, we assess why the time to reach steady state in the CH<sub>3</sub>OH/C<sub>2</sub>H<sub>5</sub>OH production is so strongly dependent on the plasma power.

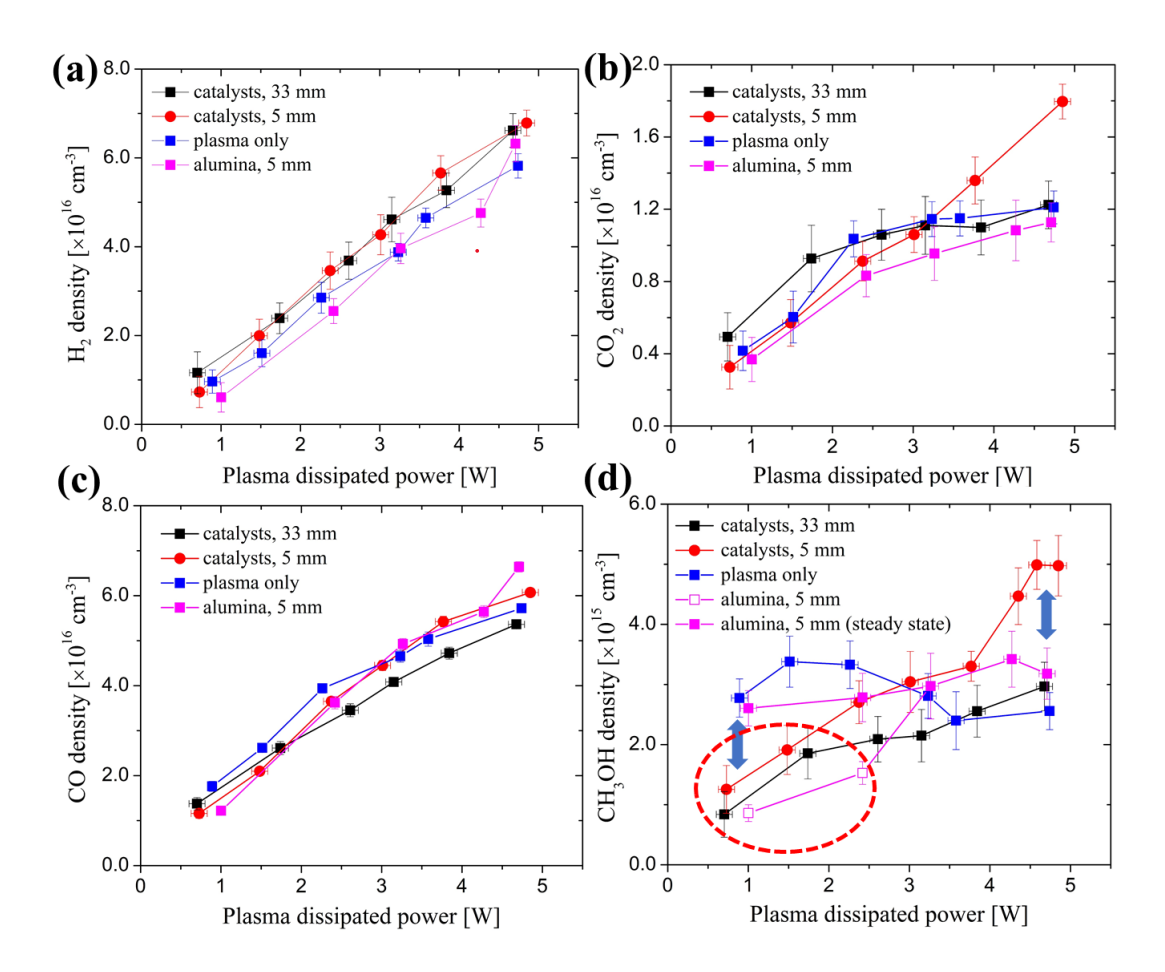


**Figure 5.** Product densities as a function of plasma dissipated power for identical experimental conditions as reported in Figure 4: (a) H<sub>2</sub> density (b) CO density (c) CO<sub>2</sub> density (d) CH<sub>3</sub>OH/C<sub>2</sub>H<sub>5</sub>OH density. The data encircled in the red dashed line in subfigure (d) is impacted by non-steady state effects and the blue arrow indicates the observed plasma-catalyst synergy.

### 4. Absorption of methanol/ethanol on catalyst substrate

The vapor pressure of methanol and ethanol at  $20^{\circ}$  is 94 and 44 mmHg [25]respectively corresponding to 6 and 12% which larger than the original reactants concentration, hence there will not be significant condensation in the reactor even without additional heating. Examples of time-resolved mass spectrometer signals at m/z = 31 amu corresponding to methanol/ethanol after

switching off the plasma are shown in figure 6. Figure 3(a) shows that this minutes-long decay is found for CH<sub>3</sub>OH/C<sub>2</sub>H<sub>5</sub>OH but not for CO. The 'plasma only' case in Figure 6 shows that once the plasma is switched off, the production of CH<sub>3</sub>OH/C<sub>2</sub>H<sub>5</sub>OH stops and the MS signals decrease on a timescale of a few milliseconds suggesting negligible accumulation of CH<sub>3</sub>OH/C<sub>2</sub>H<sub>5</sub>OH on the quartz capillary wall. However, in the presence of catalyst and alumina particles, the MS signal decreases on a time scale of minutes, orders of magnitude larger than the gas residence time in the system, suggesting another source of CH<sub>3</sub>OH/C<sub>2</sub>H<sub>5</sub>OH is present after switching off the plasma.

This additional source of methanol/ethanol is due to desorption of previously adsorbed CH<sub>3</sub>OH/C<sub>2</sub>H<sub>5</sub>OH onto the particles in the reactor as the phenomenon is also observed for alumina particles which cannot serve as catalysts. This conclusion is further supported by several publications reporting the possibility of CH<sub>3</sub>OH/C<sub>2</sub>H<sub>5</sub>OH absorption on catalysts or Al<sub>2</sub>O<sub>3</sub> support [29]–[31]. Therefore, the various decay times for different conditions are impacted by changes in desorption. In addition, the comparison between the decay curves for catalysts and alumina for the same plasma dissipated power in Figure 6 suggests that it requires a shorter time to remove the absorbed CH<sub>3</sub>OH/C<sub>2</sub>H<sub>5</sub>OH molecules from alumina particles than from catalyst particles under the investigated experimental conditions.

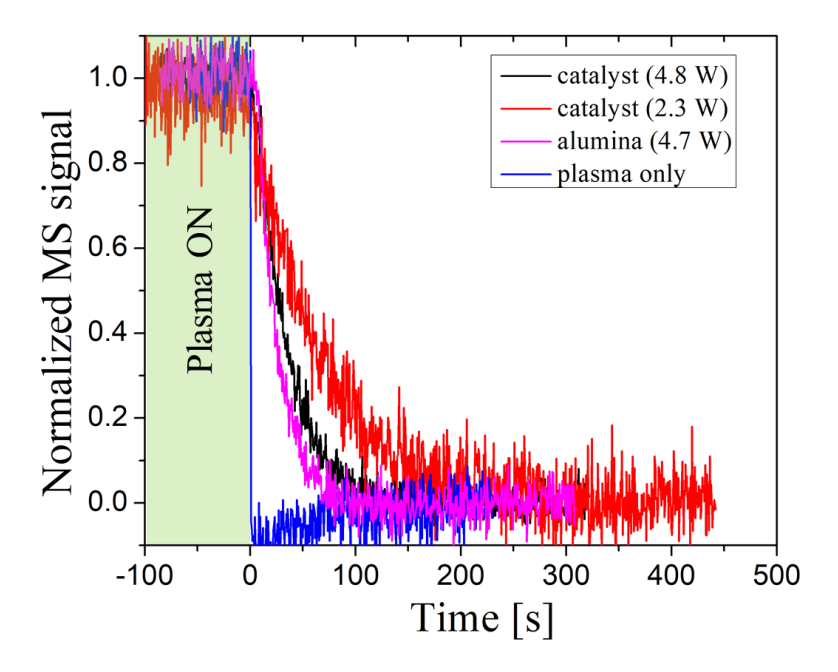


**Figure 6.** Time-resolved normalized MS signal at 31 amu attributed to methanol/ethanol after switching off the plasma at t=0 s for configuration A (Figure 1). The accuracy of the power measurement is 0.1 W.

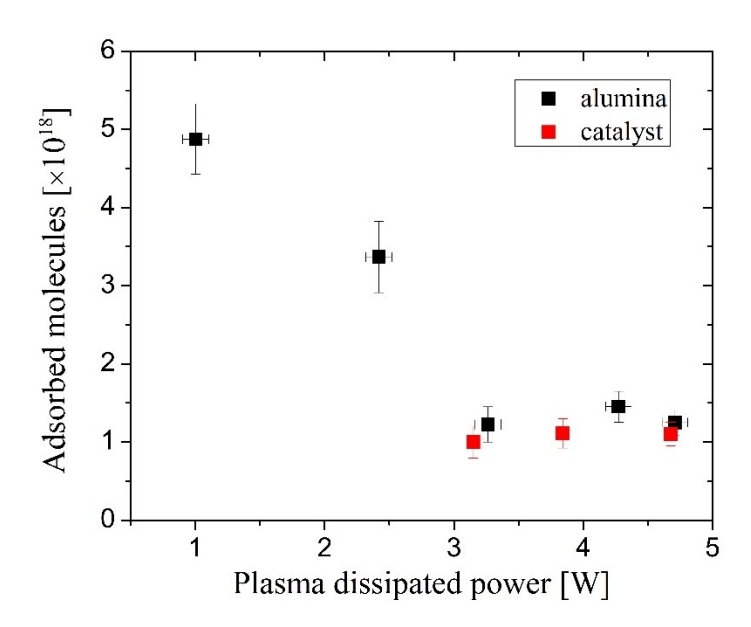


**Figure 7.** Amount of absorbed methanol/ethanol molecules on the surface of the catalyst and alumina particles during steady-state plasma effluent exposure as a function of plasma dissipated power for a distance of 33 mm between plasma and catalyst. The measurements are conducted after steady-state operation of the reactor is achieved.

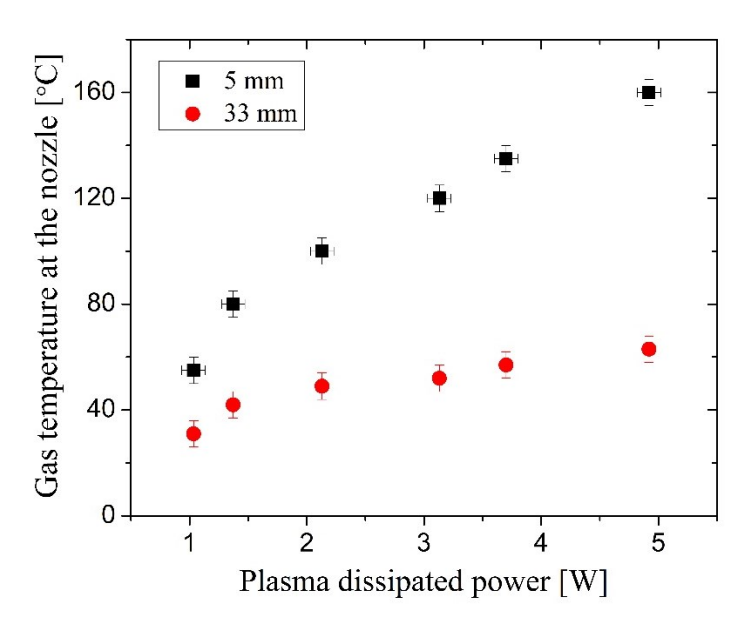
The area under the decay curve in Figure 6 is the total amount of CH<sub>3</sub>OH/C<sub>2</sub>H<sub>5</sub>OH molecules desorbed from the particles after the plasma is switched off and hence is a measure of theamount of surface adsorbed molecules during steady-state exposure by the plasma effluent. Figure 7 shows this total amount of absorbed molecules on the particle surface as a function of plasma dissipated power. The amount of absorbed molecules at small plasma powers (~1 W) is about 5 times larger than the higher plasma power (> 3 W). The 5 times larger amount of surface molecules for low plasma powers might contribute to the longer time it takes to reach a steady state surface coverage. Figure 7 also shows that the absorption abilities of catalysts and alumina particles are similar which might suggest the dominant contribution of the alumina substrate to the observed CH<sub>3</sub>OH/C<sub>2</sub>H<sub>5</sub>OH absorption.

The observed change in the absorption ability of particles might be due to the change in gas temperature or plasma-produced reactive species as both scale with the plasma dissipated power.

Considering that the absorption ability is also significantly impacted for the plasma at 33 mm from the catalytic reaction (see figure 7), it is unlikely that radicals play a dominant role in this effect and hence it must be due to long-lived reactive species or gas heating.

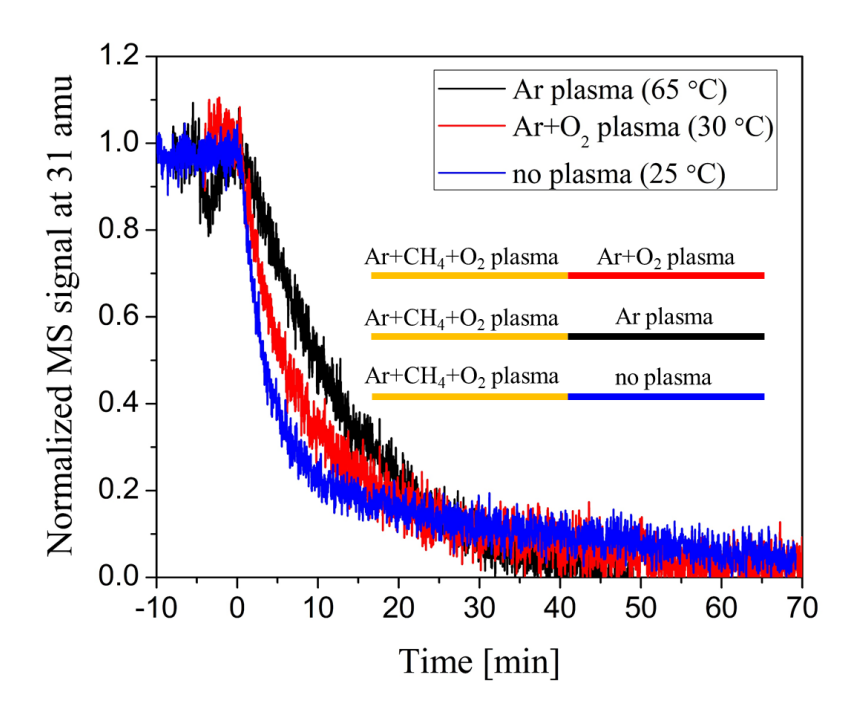
The gas temperatures at the nozzle of the quartz capillary (corresponding to the entrance of the catalytic reactor) are shown for an electrode-nozzle distance of 5 and 33 mm as a function of plasma dissipated power in figure 8. While the gas temperature increases by more than 100°C for the 5 mm distance case, the gas temperature for the 33 mm case does not increase more than 30°C. Hence, the variation in surface coverage for the 33 mm case, if due to temperature must be caused by a mere increase in gas temperature of 30°C.

Figure 9 shows the evolution of m/z=31 signals after the Ar-CH<sub>4</sub>-O<sub>2</sub> plasma is switched off for different sequential plasma exposures to evaluate the influence of gas temperature and plasma-produced species on the desorption. All three cases shown in Figure 9 have the same initial conditions, that is, the starting number of absorbed methanol molecules on the particle surface is the same. Note that the area under the curves is also the same within the experimental accuracy and hence no new sources of methanol are introduced by introducing the additional post plasma treatments during the desorption process.



**Figure 8.** Gas temperature as measured at the nozzle of the quartz capillary with a thermocouple as a function of plasma dissipated power for an electrode to nozzle distance of 5 and 33 mm.

As the MS measures the desorbed methanol and the net desorption rate will be fixed at a given temperature, the slopes of the MS signal are a measure of the surface coverage and hence the time constant (inverse of the initial slope) yields a measure of the methanol desorption time. As the argon plasma does not produce reactive species with a lifetime exceeding or similar to the gas residence time in the quartz capillary, it can be concluded from the enhanced CH<sub>3</sub>OH/C<sub>2</sub>H<sub>5</sub>OH signal the first 20 minutes after switching off the plasma that gas heating of 30 - 40 °C is able to significantly impact methanol desorption. This is further confirmed by comparing the desorption of CH<sub>3</sub>OH/C<sub>2</sub>H<sub>5</sub>OH during the exposure of the catalyst to the effluent of a low temperature Ar + O<sub>2</sub> plasma (Figure 9) operating at 30 °C which has a significantly smaller impact on the methanol desorption than the Ar plasma case at 65 °C. The results shown in figure 9 suggests that small temperature variations are more dominantly contributing to the desorption of methanol than long-lived plasma-produced species such as O<sub>3</sub> or O<sub>2</sub>( $a^1\Delta_g$ ). These results further suggest that small plasma-induced gas temperature increases even as low as 20 °C (and corresponding surface temperature increase of the catalyst and substrate) can impact species desorption and hence potentially impact conversion rates in plasma catalysis.



**Figure 9.** Time-resolved MS signal at 31 amu attributed to methanol/ethanol after switching off the Ar + 1% CH<sub>4</sub> + 0.5% O<sub>2</sub> plasma at t=0s for different post plasma exposure conditions during

the desorption phase: Ar plasma, Ar + 1% CH<sub>4</sub> + 0.5% O<sub>2</sub> gas flow (no plasma) and Ar+ 0.5% O<sub>2</sub> plasma yielding a gas temperature at the entrance of the catalytic reactor of 65 °C, 25 °C and 30 °C respectively.

## 5. Correlation between plasma-produced reactive species and methanol/ethanol production

In the previous section, we showed that the plasma-catalyst combination can impact desorption rates and CH<sub>3</sub>OH/C<sub>2</sub>H<sub>5</sub>OH yields particularly at low plasma powers. In this section, we analyze the synergistic enhancement in methanol production as reported in figure 5(d), at high plasma powers for steady-state conditions in more detail. The largest increase in methanol production found for the investigated conditions in this study is 60% compared to the 'plasma only' case. This corresponds to an increase of the absolute density of methanol of ~2×10<sup>15</sup> cm<sup>-3</sup>. While this synergistic effect is moderate and insufficient to be valuable from an application perspective, the controlled decoupled plasma-catalysis experiments in this study provide an excellent opportunity to contribute to a more detailed understanding of the observed synergistic effect in plasma catalysis applications based on detailed experiments.

We measured the reactive species by MBMS implementing another 50 Hz modulation onto the plasma to enable the accurate subtraction of the background [15]. While several radicals were probed, we were only able to measure a radical species at a mass of 15 amu corresponding to the mass of CH<sub>3</sub><sup>+</sup> and 47 amu corresponding to CH<sub>3</sub>O<sub>2</sub><sup>+</sup>. Figure 10 (a) presents a time-resolved measurement of CH<sub>3</sub><sup>+</sup> with the electron energy of the ionizer of 12.5 eV at a plasma power of 5 W for an electrode to nozzle distance of 5 mm. Significant differences can be found between the 'plasma on' and 'plasma off' periods, indicating the existence of a radical species. The electron energy of 12.5 eV was chosen to be sufficiently above the ionization energy of the CH<sub>3</sub> radical (9.8 eV) and low enough to avoid the contribution of CH<sub>3</sub><sup>+</sup> formed by dissociative ionization of CH<sub>4</sub> molecules which requires an electron energy of 14.0 eV [32]. In addition, the contributions of CH<sub>3</sub><sup>+</sup> from other stable products like CH<sub>3</sub>OH can be excluded as the measured signal dramatically dropped down below the detection limit when increasing the distance between the plasma to the MBMS orifice by only 1 mm.

Assuming the measured species is CH<sub>3</sub>, an absolute calibration with CH<sub>4</sub>, resulting in an absolute density of the order of  $\sim 10^{14}$  cm<sup>-3</sup>. This seems however inconsistent with the kinetics of CH<sub>3</sub> and the CH<sub>3</sub> lifetime. The production reactions of CH<sub>3</sub> in the plasma afterglow was previously shown

to be negligible compared to the destruction reactions [10] and the lifetime of CH<sub>3</sub> in the afterglow region can be estimated according to the dominant destruction reaction for the investigated experimental conditions [10]

$$CH_3 + O_2 + M \rightarrow CH_3O_2 + M, k_1 = 9.79 \times 10^{-31} \text{ cm}^6 \text{ s}^{-1}.$$
 (R2)

Assuming the gas temperature is 400 K and the O<sub>2</sub> density is depleted by 50% in the plasma, yields a lifetime for CH<sub>3</sub> of ~1 µs. This lifetime is significantly smaller than the time needed to transition the suction region of the mass spectrometer (~18 µs) [15] and hence the CH<sub>3</sub> density should drop below the MBMS detection limit before entering the molecular beam. The measurement hence suggests that the measured MS signal at 15 amu is due to a reactive species with a lifetime between 10 μs to a few ms at most (gas residence time corresponding to a gas plug of 1 mm in the reactor). We can further exclude the possibility of vibrationally excited CH<sub>4</sub> because its lifetime is even shorter than CH<sub>3</sub> [33]. CH<sub>3</sub>O<sub>2</sub>, which was detected at m/z=41 amu, is identified as the most abundant radical in kinetic models of CH<sub>4</sub>-O<sub>2</sub> plasma [10] and is the most likely candidate. Unfortunately, the data regarding the electron impact ionization (EII) cross-section of CH<sub>3</sub>O<sub>2</sub> is not reported to our knowledge and a quantitative study would require chemical ionization or photoionization [18],[34] which is not a capability of the MBMS used. Fu et al. [18] reported that the CH<sub>3</sub>O<sub>2</sub><sup>+</sup> ion might be unstable and likely decomposes into CH<sub>3</sub><sup>+</sup> and O<sub>2</sub> depending on the excess energy during the ionization process. The calculated ionization potential of CH<sub>3</sub>O<sub>2</sub> was 10.8 eV and the extra energy available from the 12.5 eV electrons in the ionizer would dissociate CH<sub>3</sub>O<sub>2</sub><sup>+</sup> to yield CH<sub>3</sub><sup>+</sup>. Meloni et al. [19] measured the photoionization efficiency curve for CH<sub>3</sub>O<sub>2</sub>, yielding adiabatic ionization energy of CH<sub>3</sub>O<sub>2</sub> to be (10.33±0.05 eV) and a CH<sub>3</sub><sup>+</sup>– O<sub>2</sub> bond energy of 0.83±0.07 eV. The above information would suggest a threshold energy of (11.2-11.5 eV) to produce CH<sub>3</sub><sup>+</sup> from CH<sub>3</sub>O<sub>2</sub>. This is consistent with our experimental findings showing that the CH<sub>3</sub><sup>+</sup> signal was close to the detection limit for electron energy of 12.0 eV. The significant difference in CH<sub>3</sub><sup>+</sup> signals measured at 12.0 eV and 12.5 eV is more consistent with a species having a threshold ionization of 12.0 eV rather than 9.84 eV like CH<sub>3</sub>. The ratio of the electronimpact ionization cross sections of CH<sub>3</sub> forming CH<sub>3</sub><sup>+</sup> at 12.0 eV and 12.5 eV is only 0.8 consistent with the interpretation of the MS signal at 15 amu to be due to CH<sub>3</sub>O<sub>2</sub>. As the CH<sub>3</sub>O<sub>2</sub> signal is more than one order of magnitude smaller than m/z=31, likely due to the reported unstable nature of the CH<sub>3</sub>O<sub>2</sub><sup>+</sup> ion [18], we estimate the CH<sub>3</sub>O<sub>2</sub> density from the m/z=31 signal.

While there is no partial EII cross-section for CH<sub>3</sub><sup>+</sup> formation from CH<sub>3</sub>O<sub>2</sub> available in the literature, we can still make an approximate estimation of the CH<sub>3</sub>O<sub>2</sub> density assuming the EII cross-section is the same as for CH<sub>3</sub>OH although with correction for the ionization threshold. The threshold energy to produce CH<sub>3</sub><sup>+</sup> from CH<sub>3</sub>OH is about 13.8 eV, and the EII cross-section is about 2×10<sup>-18</sup> cm<sup>2</sup> at 15.0 eV [20]. Assuming a similar EII cross-section for CH<sub>3</sub><sup>+</sup> formation from CH<sub>3</sub>O<sub>2</sub> would yield the highest CH<sub>3</sub>O<sub>2</sub> density in Figure 10(b) to be 2×10<sup>15</sup> cm<sup>-3</sup> with a calibration using CO<sub>2</sub> (m/z=44). Although this density estimation has large uncertainties, it suggests that the measurement is consistent with a density of CH<sub>3</sub>O<sub>2</sub> on the order of 10<sup>15</sup> cm<sup>-3</sup>.

If CH<sub>3</sub>O<sub>2</sub> is the dominant radical in the afterglow region, its lifetime can be estimated according to its self-recombination reaction since its reaction with CH<sub>4</sub> or other long-lived molecules is very slow:

$$CH_3O_2 + CH_3O_2 \rightarrow CH_3OH + CH_2O + O_2, k_4 = 2.19 \times 10^{-13} \text{ cm}^3 \text{ s}^{-1},$$
 (R3)

$$CH_3O_2 + CH_3O_2 \rightarrow 2CH_3O + O_2, k_5 = 1.29 \times 10^{-13} \text{ cm}^3 \text{ s}^{-1}.$$
 (R4)

The lifetime is estimated to be 1.4 ms if assuming a CH<sub>3</sub>O<sub>2</sub> density of  $2\times10^{15}$  cm<sup>-3</sup> equal to the observed increase in the absolute density of methanol by the plasma catalyst interaction. This lifetime is likely an overestimation as we neglected its reaction with other radicals such as H, O or OH. All the above analysis suggests that a density of CH<sub>3</sub>O<sub>2</sub> on the order of  $10^{15}$  cm<sup>-3</sup> with a lifetime of the order of  $\sim1$  ms are consistent with our MBMS measurements.

Figure 10(b) shows the MS signal at 15 amu attributed to CH<sub>3</sub>O<sub>2</sub> at the inlet of the catalytic reactor and the increase in methanol/ethanol density at the outlet of the catalytic reactor as a function of plasma power. The trends of both the CH<sub>3</sub><sup>+</sup> MS signal attributed to CH<sub>3</sub>O<sub>2</sub> and methanol/methanol correlate well. In addition, the CH<sub>3</sub><sup>+</sup> signal is below the detection limit for plasma powers less than 4 W, consistent with the lack of increase in methanol compared to the plasma only case suggesting that only for cases with a detectible amount of CH<sub>3</sub>O<sub>2</sub> an enhancement of the methanol formation by the catalyst was found. This correlation suggests that CH<sub>3</sub>O<sub>2</sub> might play a key role in the production of CH<sub>3</sub>OH on the surface of the catalyst.

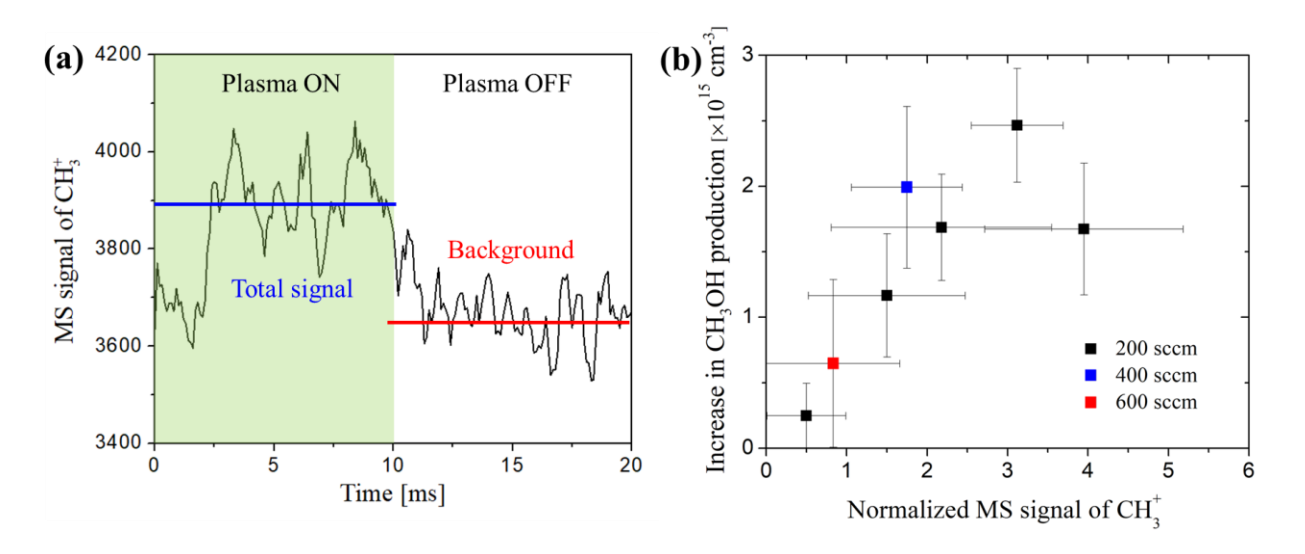


**Figure 10.** (a) Time-resolved MS signals of CH<sub>3</sub><sup>+</sup> attributed to CH<sub>3</sub>O<sub>2</sub> (see text for details) for a plasma power of 4.7 W and an electrode to nozzle-distance of 5 mm; (b) Correlation between the CH<sub>3</sub>O<sub>2</sub> radical flux at the nozzle and the increase in CH<sub>3</sub>OH production in the catalyst reactor for variations in plasma dissipated power and gas flow rate.

Nonetheless, gas temperatures also vary with power as shown in Figure 8. At a distance of 5 mm, the gas temperature can reach 160 °C at 5 W. The resulting elevation of the catalyst temperature might be able to trigger thermal catalysis which could enhance methanol production. To assess this effect, the impact of gas flow rates on the methanol production, gas temperature and radical density was measured. Figure 11 (a) shows that while the methanol density remains constant as a function of the gas flow rate for the plasma only case (resulting in a linear increase in methanol production as a function of gas flow rate), a reduction in the methanol/ethanol density with increasing gas flow rate was observed when the catalyst is present. This decrease in methanol/ethanol density results in the lack of a significant observed synergistic effect at a flow rate of 600 sccm. However, this effect can be further enhanced by the reduced gas residence time.

Figure 11(b) shows the corresponding gas temperatures and MS signals of CH<sub>3</sub>O<sub>2</sub>. The gas temperature reduces from 160 °C to about 100 °C and the CH<sub>3</sub>O<sub>2</sub> signal decreases about 70% with increasing gas flow rate from 200 sccm to 600 sccm. The similar trends do not allow to make a conclusion of the cause of the reduction in methanol-based from this data alone but a comparison with another condition at the same gas temperature provides more insights. The 400 sccm case has

a gas temperature of about 125 °C and the synergistic effect was observed. This case has the same gas temperature as the reported results between 3 and 4 W in Figure 5(d), which does not show any synergistic effect in methanol production. Hence, the observed synergistic effects can be attributed to plasma-produced species rather than gas heating.

The strong correlation both for the power and gas flow variation between the CH<sub>3</sub>O<sub>2</sub> signal and the CH<sub>3</sub>OH (see figure 10 b) suggests the dominant role of radicals and in particular radicals with lifetimes between 100µs and 1 ms like CH<sub>3</sub>O<sub>2</sub>.

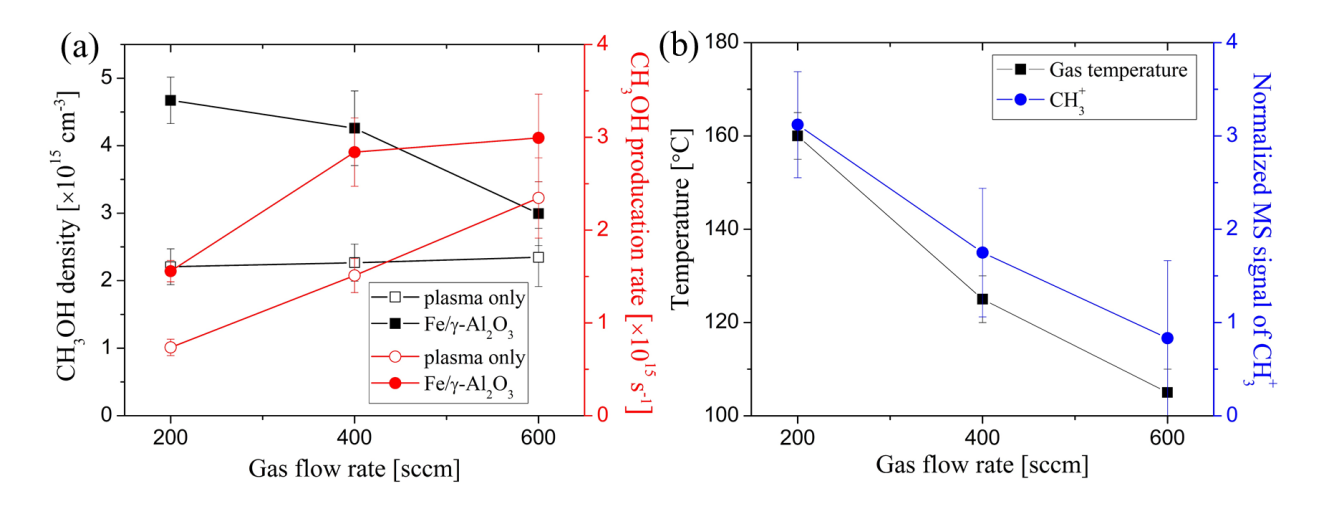


**Figure 11.** Impact of the gas flow rate on (a) the CH<sub>3</sub>OH density and production rates and (b) the gas temperature and MS signal of CH<sub>3</sub><sup>+</sup> attributed to CH<sub>3</sub>O<sub>2</sub> at a fixed plasma dissipated power of 4.7 W±0.1 W.

### 6. Possible reaction pathways underpinning observed synergy.

Yi et al [11] previously suggested that the production of CH<sub>3</sub>OH on plasma-exposed catalyst could be attributed to the reaction between chemisorbed oxygen species with the plasma-produced CH<sub>3</sub> radicals to form CH<sub>3</sub>O adsorbed to the catalytic surface. In the present study, this proposed mechanism is not able to explain the observed results in view of the sub-microsecond lifetime of the CH<sub>3</sub> radical. Nevertheless, another reaction pathway including the CH<sub>3</sub>O<sub>2</sub> radicals is a more likely candidate to explain the increased CH<sub>3</sub>OH production. For example, in the gas-phase plasma, the self-recombination of CH<sub>3</sub>O<sub>2</sub> would lead to the formation of CH<sub>3</sub>O radicals via R3-R4, which can chemisorb on the catalytic surface as CH<sub>3</sub>O<sub>ad</sub> yielding the same surface chemistry without the requirement of CH<sub>3</sub> radicals.

Furthermore, surface chemistry to form methanol from CH<sub>3</sub>O<sub>ad</sub> was proposed to involve H radicals [11]. If the reaction between H + CH<sub>3</sub>O<sub>ad</sub> is indeed responsible for the production of CH<sub>3</sub>OH on the catalyst surface, the H density should be at least similar to the observed increase in methanol  $\sim 2 \times 10^{15}$  cm<sup>-3</sup>, the detection limit of the MBMS [35]. This is highly unlikely as the lifetime of H is about  $\sim 2$  µs (considering R2 and the three-body reaction between H and O<sub>2</sub> with a CH<sub>3</sub>O<sub>2</sub> density of at least  $2 \times 10^{15}$  cm<sup>-3</sup>). The diffusion timescale of H over a distance of 20 µm is on the order of 4 µs according to the diffusion coefficients taken from [22], which will lead to a large amount of gas phase recombination of H radicals before reaching the catalyst. This suggests that H cannot be responsible for the observed synergistic plasma-catalyst effect. One possibility is that CH<sub>3</sub>O<sub>ad</sub> can react with itself to produce CH<sub>3</sub>OH, like the equivalent gas-phase reaction:

$$CH_3O + CH_3O \rightarrow CH_2O + CH_3OH, k_6 = 1.0 \times 10^{-10} \text{ cm}^3 \text{ s}^{-1}.$$
 (R6)

Alternatively, reactions of CH<sub>3</sub>O<sub>ad</sub> with H<sub>2</sub>, similar to their gas-phase equivalent might be possible if they would proceed at a higher rate than in the gas phase.

Agarwal et al. [36] investigated aqueous selective CH<sub>4</sub> catalytic oxidation to CH<sub>3</sub>OH and demonstrated that adding O<sub>2</sub> to the reaction mixture would produce CH<sub>3</sub>O<sub>2</sub> radicals by reacting with CH<sub>3</sub> radicals. The proposed reaction pathway suggests the importance of CH<sub>3</sub>O<sub>2</sub> radicals to enhance oxygenates' production in surface reactions although for completely different reaction conditions. While the detailed mechanism is subject to further study, these results suggest a viable pathways through CH<sub>3</sub>O<sub>2</sub> for methanol/ethanol production.

While recognizing that this study was performed in a reactor in which the catalyst particles were not in direct contact with the active plasma, an important outcome of this study is the large impact of transport limitations that might also play an important role for packed bed reactors where the catalyst is in 'direct contact' with the plasma. These transport limitations have been largely ignored by the research community when proposing surface reaction mechanisms in many plasma-catalysis studies. Even when a surface-hugging plasma might be in direct contact with the surface, a sheath will be present which depletes electrons near the interface of the catalyst and hence also radical production requiring radicals produced in the bulk plasma to diffuse through a sheath region. As a typical sheath thickness at atmospheric pressure is of the order of  $100 \mu m$  [37], this requires a diffusion time of the order of  $10 to 100 \mu s$  for H and CH<sub>3</sub> at 400 to 100 to 100

contribute to plasma-catalyst interactions. We showed in this work that plasma-catalyst synergy is possible due to long-lived radical species such as alkylperoxy radicals with lifetimes comparable or larger than these diffusive timescales. While these species might be less reactive in the gas phase they can still play an important role in plasma catalysis as they are less impacted by transport limitations on the typical length scales between pellets of hundreds of micrometers in pack-bed reactors.

#### 7. Conclusion

In this work, the mechanisms underpinning the interaction of plasma with Fe/γ-Al<sub>2</sub>O<sub>3</sub> catalyst in the context of direct conversion of methane to CO, CO<sub>2</sub> and oxygenates at room temperature are investigated by incorporating the catalyst reactor downstream of the plasma jet. An enhancement of CH<sub>3</sub>OH in the presence of a catalyst compared to the plasma only case is observed for the shortest distance between the plasma and catalyst studied in this work. Correlations between MBMS measurements and estimates of species lifetimes suggest that this synergistic effect is caused by radical species most likely CH<sub>3</sub>O<sub>2</sub>. It was possible to exclude dominant contributions of plasma-enabled heating on methanol formation for the synergistic effect observed in this work while it was shown that gas heating even as low as 30-40 °C was significantly impacting desorption rates of CH<sub>3</sub>OH on alumina particles. While most studies in plasma catalysis seem to focus on Elay-Rideal reactions by primary radicals such as H and CH<sub>3</sub>, this study shows that surface reactions induced by secondary more long-lived radicals such as alkylperoxy radicals might be less impacted by transport limitations and their role in surface reactions might deserve more attention.

#### **Acknowledgments**

This material is based upon work supported by the National Science Foundation (CBET 1703439). The work has significantly benefited from methods and techniques developed in the framework of work supported by the US Department of Energy, Office of Science, Office of Fusion Energy Sciences General Plasma Science program under award number DE-SC0020232 and DE-SC0001939.

## Reference

[1] Ravi, M.; Ranocchiari, M.; van Bokhoven, J. A. The Direct Catalytic Oxidation of Methane

- to Methanol-A Critical Assessment. Angew. Chemie Int. Ed. 2017, 56 (52), 16464–16483.
- [2] Joghee, P.; Malik, J. N.; Pylypenko, S.; O'Hayre, R. A Review on Direct Methanol Fuel Cells–In the Perspective of Energy and Sustainability. *MRS Energy Sustain.* **2015**, *2* (1), 3.
- [3] Larkin, D. W.; Lobban, L. L.; Mallinson, R. G. The Direct Partial Oxidation of Methane to Organic Oxygenates Using a Dielectric Barrier Discharge Reactor as a Catalytic Reactor Analog. *Catal. Today* **2001**, *71* (1–2), 199–210.
- [4] Bogaerts, A.; Tu, X.; Whitehead, J. C.; Centi, G.; Lefferts, L.; Guaitella, O.; Azzolina-Jury, F.; Kim, H.-H.; Murphy, A. B.; Schneider, W. F.; et al. The 2020 Plasma Catalysis Roadmap. *J. Phys. D. Appl. Phys.* **2020**, *53* (44), 443001.
- [5] Nozaki, T.; Okazaki, K. Non-Thermal Plasma Catalysis of Methane: Principles, Energy Efficiency, and Applications. *Catal. Today* **2013**, *211*, 29–38.
- [6] Kim, J.; Go, D. B.; Hicks, J. C. Synergistic Effects of Plasma-Catalyst Interactions for CH 4 Activation. *Phys. Chem. Chem. Phys.* **2017**, *19* (20), 13010–13021.
- [7] Kim, J.; Abbott, M. S.; Go, D. B.; Hicks, J. C. Enhancing C-H Bond Activation of Methane via Temperature-Controlled, Catalyst-Plasma Interactions. *ACS Energy Lett.* **2016**, *1* (1), 94–99.
- [8] Astafan, A.; Batiot-Dupeyrat, C.; Pinard, L. Mechanism and Kinetic of Coke Oxidation by Nonthermal Plasma in Fixed-Bed Dielectric Barrier Reactor. *J. Phys. Chem. C* **2019**, *123* (14), 9168–9175.
- [9] Chawdhury, P.; Wang, Y.; Ray, D.; Mathieu, S.; Wang, N.; Harding, J.; Bin, F.; Tu, X.; Subrahmanyam, C. A Promising Plasma-Catalytic Approach towards Single-Step Methane Conversion to Oxygenates at Room Temperature. *Appl. Catal. B Environ.* **2021**, *284*, 119735.
- [10] De Bie, C.; Van Dijk, J.; Bogaerts, A. The Dominant Pathways for the Conversion of Methane into Oxygenates and Syngas in an Atmospheric Pressure Dielectric Barrier Discharge. *J. Phys. Chem. C* **2015**, *119* (39), 22331–22350.
- [11] Yi, Y.; Li, S.; Cui, Z.; Hao, Y.; Zhang, Y.; Wang, L.; Liu, P.; Tu, X.; Xu, X.; Guo, H.; et al. Selective Oxidation of CH<sub>4</sub> to CH<sub>3</sub>OH through Plasma Catalysis: Insights from Catalyst Characterization and Chemical Kinetics Modelling. *Appl. Catal. B Environ.* **2021**, *296*, 120384.
- [12] Lustemberg, P. G.; Palomino, R. M.; Gutiérrez, R. A.; Grinter, D. C.; Vorokhta, M.; Liu, Z.; Ramírez, P. J.; Matolín, V.; Ganduglia-Pirovano, M. V.; Senanayake, S. D.; et al. Direct Conversion of Methane to Methanol on Ni-Ceria Surfaces: Metal-Support Interactions and Water-Enabled Catalytic Conversion by Site Blocking. *J. Am. Chem. Soc.* **2018**, *140* (24), 7681–7687.
- [13] Li, Y.; Jiang, J.; Hinshelwood, M.; Zhang, S.; Bruggeman, P.; Oehrlein, G. S. Characterization of Plasma Catalytic Decomposition of Methane: Role of Atomic O and Reaction Mechanism. *J. Phys. D. Appl. Phys.* **2021**, *accepted*.
- [14] Hofmann, S.; van Gessel, A. F. H.; Verreycken, T.; Bruggeman, P. Power Dissipation, Gas

- Temperatures and Electron Densities of Cold Atmospheric Pressure Helium and Argon RF Plasma Jets. *Plasma Sources Sci. Technol.* **2011**, *20* (6), 065010.
- [15] Jiang, J.; Luo, Y.; Moldgy, A.; Aranda Gonzalvo, Y.; Bruggeman, P. J. Absolute Spatially and Time-resolved O, O<sub>3</sub>, and Air Densities in the Effluent of a Modulated RF-driven Atmospheric Pressure Plasma Jet Obtained by Molecular Beam Mass Spectrometry. *Plasma Process. Polym.* **2020**, *17* (6), 1900163.
- [16] Baiocchi, F. A.; Wetzel, R. C.; Freund, R. S. Electron-Impact Ionization and Dissociative Ionization of the CD<sub>3</sub> and CD<sub>2</sub> Free Radicals. *Phys. Rev. Lett.* **1984**, *53* (8), 771–774.
- [17] Itikawa, Y.; Ichimura, A.; Onda, K.; Sakimoto, K.; Takayanagi, K.; Hatano, Y.; Hayashi, M.; Nishimura, H.; Tsurubuchi, S. Cross Sections for Collisions of Electrons and Photons with Oxygen Molecules. *J. Phys. Chem. Ref. Data* **1989**, *18* (1), 23–42.
- [18] Fu, H. B.; Hu, Y. J.; Bernstein, E. R. Generation and Detection of Alkyl Peroxy Radicals in a Supersonic Jet Expansion. *J. Chem. Phys.* **2006**, *125* (1), 014310.
- [19] Meloni, G.; Zou, P.; Klippenstein, S. J.; Ahmed, M.; Leone, S. R.; Taatjes, C. A.; Osborn, D. L. Energy-Resolved Photoionization of Alkylperoxy Radicals and the Stability of Their Cations. *J. Am. Chem. Soc.* **2006**, *128* (41), 13559–13567.
- [20] Nixon, K. L.; Pires, W. A. D.; Neves, R. F. C.; Duque, H. V.; Jones, D. B.; Brunger, M. J.; Lopes, M. C. A. Electron Impact Ionisation and Fragmentation of Methanol and Ethanol. *Int. J. Mass Spectrom.* 2016, 404, 48–59.
- [21] Zawadzki, M. Electron-Impact Ionization Cross Section of Formic Acid. *Eur. Phys. J. D* **2018**, 72 (1), 12.
- [22] Vacher, J. R.; Jorand, F.; Blin-Simiand, N.; Pasquiers, S. Partial Ionization Cross-Sections of Acetone and 2-Butanone. *Int. J. Mass Spectrom.* **2008**, *273* (3), 117–125.
- [23] Możejko, P. Calculations of Electron Impact Ionization Cross Section for Simple Biomolecules: Formic and Acetic Acids. *Eur. Phys. J. Spec. Top. 2007 1441* **2007**, *144* (1), 233–237.
- [24] Große-Kreul, S.; Hübner, S.; Schneider, S.; Ellerweg, D.; von Keudell, A.; Matejčík, S.; Benedikt, J. Mass Spectrometry of Atmospheric Pressure Plasmas. *Plasma Sources Sci. Technol.* **2015**, *24* (4), 044008.
- [25] NIST. Standard Reference Database 69: NIST Chemistry WebBook; National Institute of Standards and Technology, 2010.
- [26] Loenders, B.; Engelmann, Y.; Bogaerts, A. Plasma-Catalytic Partial Oxidation of Methane on Pt(111): A Microkinetic Study on the Role of Different Plasma Species. *J. Phys. Chem. C* **2021**, *125* (5), 2966–2983.
- [27] Eckert, Z.; Tsolas, N.; Togai, K.; Chernukho, A.; Yetter, R. A.; Adamovich, I. V. Kinetics of Plasma-Assisted Oxidation of Highly Diluted Hydrocarbon Mixtures Excited by a Repetitive Nanosecond Pulse Discharge. *J. Phys. D. Appl. Phys.* **2018**, *51* (37), 374002.
- [28] Golda, J.; Biskup, B.; Layes, V.; Winzer, T.; Benedikt, J. Vacuum Ultraviolet Spectroscopy

- of Cold Atmospheric Pressure Plasma Jets. Plasma Process. Polym. 2020, 17 (6), 1900216.
- [29] Greenler, R. G. Infrared Study of the Adsorption of Methanol and Ethanol on Aluminum Oxide. *J. Chem. Phys.* **1962**, *37* (9), 2094–2100.
- [30] Korhonen, S. T.; Bañares, M. A.; Fierro, J. L. G.; Krause, A. O. I. Adsorption of Methanol as a Probe for Surface Characteristics of Zirconia-, Alumina-, and Zirconia/Alumina-Supported Chromia Catalysts. *Catal. Today* **2007**, *126* (1–2), 235–247.
- [31] Schauermann, S.; Hoffmann, J.; Johánek, V.; Hartmann, J.; Libuda, J. Adsorption, Decomposition and Oxidation of Methanol on Alumina Supported Palladium Particles. *Phys. Chem. Chem. Phys.* **2002**, *4* (15), 3909–3918.
- [32] Plessis, P.; Marmet, P.; Dutil, R. Ionisation and Appearance Potentials of CH<sub>4</sub> by Electron Impact. *J. Phys. B At. Mol. Phys.* **1983**, *16* (7), 1283–1294.
- [33] Nozaki, T.; Muto, N.; Kado, S.; Okazaki, K. Dissociation of Vibrationally Excited Methane on Ni Catalyst: Part 1. Application to Methane Steam Reforming. *Catal. Today* **2004**, *89* (1–2), 57–65.
- [34] Nozière, B.; Hanson, D. R. Speciated Monitoring of Gas-Phase Organic Peroxy Radicals by Chemical Ionization Mass Spectrometry: Cross-Reactions between CH<sub>3</sub>O<sub>2</sub>, CH<sub>3</sub>(CO)O<sub>2</sub>, (CH<sub>3</sub>)<sub>3</sub>CO<sub>2</sub>, and c-C<sub>6</sub>H<sub>1</sub>O<sub>2</sub>. *J. Phys. Chem. A* **2017**, *121* (44), 8453–8464.
- [35] Jiang, J.; Santosh K Kondeti, V. S.; Nayak, G.; Bruggeman, P. J. Experimental and Modeling Studies of the Plasma Chemistry in a Humid Ar Radiofrequency Atmospheric Pressure Plasma Jet. J. Phys. D. Appl. Phys. 2021, 55 (22), 225206.
- [36] Agarwal, N.; Freakley, S. J.; McVicker, R. U.; Althahban, S. M.; Dimitratos, N.; He, Q.; Morgan, D. J.; Jenkins, R. L.; Willock, D. J.; Taylor, S. H.; et al. Aqueous Au-Pd Colloids Catalyze Selective CH<sub>4</sub> Oxidation to CH<sub>3</sub>OH with O<sub>2</sub> under Mild Conditions. *Science* (80-.). **2017**, 358 (6360), 223–227.
- [37] Benedikt, J.; Hecimovic, A.; Ellerweg, D.; von Keudell, A. Quadrupole Mass Spectrometry of Reactive Plasmas. *J. Phys. D. Appl. Phys.* **2012**, *45* (40), 403001.